International Journal of Thermophysics, Vol. 28, No. 2, April 2007 (© 2007)
DOI: 10.1007/s10765-007-0150-x

Radiance Temperature and Normal Spectral Emittance (in the Wavelength Range of 1.5 to 5 μm) of Nickel at its Melting Point by a Pulse-Heating Technique

K. Boboridis,[1,2] A. Seifter,[3] A. W. Obst,[3] and D. Basak[4,5]

The radiance temperature of nickel at its melting point was measured at four wavelengths (in the nominal range of 1.5 to 5 μm) by a pulse-heating technique using a high-speed fiber-coupled four-channel infrared pyrometer. The method was based on rapid resistive self-heating of a specimen from room temperature to its melting point in less than 1 s while simultaneously measuring the radiance emitted by it in four spectral bands as a function of time. A plateau in the recorded radiance-versus-time traces indicated melting of the specimen. The melting-point radiance temperature for a given specimen was determined by averaging the temperature measured along the plateau at each wavelength. The results for several specimens were then, in turn, averaged to yield the melting-point radiance temperature of nickel, as follows: 1316 K at 1.77 μm, 1211 K at 2.26 μm, 995 K at 3.48 μm, and 845 K at 4.75 μm. The melting-point normal spectral emittance of nickel at these wavelengths was derived from the measured radiance in each spectral band using the published value of the thermodynamic (true) melting temperature of nickel.

KEY WORDS: emissivity; emittance; infrared; melting; nickel; pulse heating; pyrometry; radiance temperature.

[1] Department of Physics, University of Cyprus, P.O. Box 20537, 1678 Nicosia, Cyprus.
[2] To whom correspondence should be addressed. E-mail: kboboridis@fastmail.fm
[3] Physics Division, Los Alamos National Laboratory, Los Alamos, New Mexico 87545, U.S.A
[4] Space Systems Group, Orbital Sciences Corporation, 21839 Atlantic Blvd., Dulles, Virginia, 20166, U.S.A
[5] Metallurgy Division, National Institute of Standards and Technology, Gaithersburg, Maryland 20899, U.S.A

1. INTRODUCTION

A few years ago at the Los Alamos National Laboratory (LANL) we designed and built a new four-wavelength infrared radiation thermometer, more commonly referred to as a pyrometer, for surface-temperature measurements on shock-compressed materials [1]. Since then, this high-speed instrument has been used successfully in a variety of experimental setups, at LANL and elsewhere, providing a wealth of useful shock-physics data. At the same time, the obtained results and their often-difficult interpretation helped advance our knowledge concerning the application and the limits of pyrometry in the very demanding environment of shock-physics experimentation [2; 3].

As with any instrument, it was crucial to validate the new pyrometer before its full-scale use. Being aware of the many uncertainties that accompany pyrometric shock-temperature measurements [4], we realized that simply using a material with well-established properties in a series of shock-compression experiments would probably not supply us with accurate information on the instrument's performance. Instead, we decided to utilize a different setup that would allow us to carry out a sufficient number of (low cost) experiments without the above-mentioned uncertainties that are not inherent to pyrometry, and, more importantly, in which the measurement parameter of interest (temperature) would be highly reproducible and known.

We used the "millisecond-resolution" pulse-heating facility at the Metallurgy Division of the US National Institute of Standards and Technology (NIST) to look at the melting transition of several metals. By nature, the temperature at these transitions is constant, making the task of validating a pyrometer straightforward. Tin, zinc, aluminum, and silver were chosen to adequately cover the useful measurement range of our pyrometer with their melting points, and the results, which were very encouraging, have already been reported [5; 6]. In addition to these four metals, we also included nickel in our investigation, a metal that had been studied in the past at this same facility [7; 8], and was known to behave very well in this kind of experiment. From a sensitivity point of view, its melting point is considerably higher than the range for which our pyrometer was primarily designed. Nevertheless, it could still be measured without the need for any attenuating neutral density filters.

Aside from evaluating the pyrometer by measuring the (thermodynamic) melting temperature of nickel, which was the main purpose of this test series, we were also interested in its melting-point radiance temperature at the operating wavelengths of our pyrometer. It has long been suggested that the melting-point radiance temperatures of selected

metals be used as secondary high-temperature reference points for high-speed pyrometry [9; 10]. Extensive research in this direction has been conducted by NIST and the Italian Instituto Nazionale Ricerca Metrologica[6] (INRIM) over the past three decades. That research was focused on wavelengths in the visible and near-infrared regions up to 1.5 μm. In this paper we present our results on the melting-point radiance temperature of nickel at four wavelengths in the range of 1.5 to 5 μm. We also report its normal spectral emittance as computed from the measured radiances at the melting point and its published (true) melting temperature. In some ways, these and the data reported in Ref. [5] can be viewed as an extension of the work carried out at NIST and INRIM to lower temperatures and longer wavelengths. Finally, we discuss our findings regarding the wavelength dependence of the melting-point radiance temperature and emittance of nickel, as well as the very interesting phase (liquid/solid) dependence of the latter, which we extracted from the recorded radiances in the early stages of melting.

2. MEASUREMENT METHOD AND SYSTEM

The measurement technique is based on rapid resistive self-heating of a specimen from room temperature to its melting point in less than one second by the passage of a large electric-current pulse through it. The radiance thermally emitted by the specimen at the wavelengths of interest is measured during heating as a function of time. A plateau in the recorded radiance-versus-time traces indicates melting of the specimen.

2.1. Pulse-Heating System

The pulse-heating system consists of the specimen in series with a battery bank, an adjustable resistor, and a computer-controlled solid-state switch. The specimen is mounted inside a vacuum chamber with several ports for optical measurements. To allow measurements in the mid-infrared spectral region we used a CaF_2 window, instead of the typical BK7 window, in the pyrometry port. The battery bank voltage and the setting of the adjustable resistor determine the heating rate of the specimen. Details regarding the construction and operation of the pulse-heating circuit are given in Refs. [11; 12; 13].

[6] Formerly known as the Instituto di Metrologia "G. Colonnetti" (IMGC).

2.2. Radiometric System

The LANL pyrometer consists of two separate units, a front-optics unit and a detector unit, that are linked with an optical fiber. This modular design offers flexibility in the choice of front optics that is most suitable for a particular experiment. For the present work we used a module that utilizes a pair of 90°-off-axis parabolic mirrors to collect thermally emitted radiance from a circular spot of 1.5 mm in diameter on the specimen and focus it on the optical fiber. The radiance that is transmitted by the fiber to the detector unit is then spectrally split, using dichroic beamsplitters, into four beams and detected by an equal number of fast, LN_2-cooled InSb photodiodes. The four channels are nominally centered at 1.77, 2.27, 3.51, and 4.82 μm. Their respective spectral bandwidths (FWHM) are 0.26, 0.62, 0.74, and 1.1 μm. The blackbody-temperature threshold of the pyrometer is approximately 350 K. It is capable of measuring the radiance temperature in the four wavelength bands with a time resolution of 20 ns. However, a sampling interval of 0.1 ms per data point was sufficiently short for the melting experiments presented here. A more elaborate description of this instrument and its calibration in a slightly different configuration can be found in Ref. [1].

3. DATA REDUCTION

3.1. Radiance Temperature

For each of the four channels, the radiance temperature of a pulse-heated specimen is computed as a function of time from the ratio of the measured signal to the signal recorded during calibration with a blackbody furnace at a reference (true) temperature [5]. Because of the broad spectral bandwidth of the channels, this involves numerically solving an integral equation and requires that the relative spectral-radiance responsivity of each channel, as a function of wavelength, be known.

The melting-point radiance temperatures for a given specimen are determined by averaging the computed radiance temperatures along the melting plateau of each channel. The results from several specimens are then, in turn, averaged to determine the melting-point radiance temperatures for the metal, in this case, nickel.

The wavelength associated with the melting-point radiance temperature in each channel is the mean effective wavelength between the radiance temperature in that channel and its calibration temperature, as defined by Kostkowski and Lee [14].

All temperatures reported in this paper are consistent with the definition of the International Temperature Scale of 1990 above the silver point [15].

3.2. Normal Spectral Emittance

As described in Ref. [5], the normal spectral emittance at the melting point is determined, in each channel, from the ratio of the actual signal at the melting point to the expected signal for a blackbody at the known (true) melting temperature of the metal. By "actual signal" here, we mean the overall average of the average signals measured along the melting plateaus of several specimens.

The wavelength associated with the normal spectral emittance in each channel is the mean effective wavelength, as defined in Ref. [14], between the melting-point radiance temperature of that channel and (true) melting temperature of the metal, subject to the limitations pointed out in Ref. [5].

4. MEASUREMENTS

The measurements were performed on five nickel specimens in the form of strips that were cut from a 0.25-mm-thick foil. The strips were 50 mm in length and 7 mm in width. The exposed length of the strips, which was actually heated during the experiments, was shorter by a few millimeters because both ends were clamped in the specimen holder. As reported by the manufacturer, the nickel material was 99.98% pure by mass. According to the same report, the major typical impurities (in ppm by mass) were as follows: C, 70; Cu, Fe, Mg, Mn, Ti, and S, 10; Co, Cr, and Si, 8.

An integrating-sphere reflectometer, constructed at LANL [16], was used to measure the initial (prior to heating) normal spectral emittance of the specimens at 1.55 μm in order to reveal any possible correlation between the initial surface roughness of the specimens and the melting-point radiance temperatures. As it turned out, however, the variation among the specimens with respect to their initial emittance was very small, namely in the range of 0.244 to 0.253.

Before each measurement, the experiment chamber was evacuated to below 4 Pa and then back-filled with argon to a pressure slightly above atmospheric. This was done to reduce oxidation, as well as the rate of evaporation from the specimens [17], and as a consequence, coating of the chamber windows. The pyrometry window was carefully examined after each experiment and replaced if damage from molten specimen debris was observed.

In addition, prior to melting them, three of the specimens were subjected to a 1 s-long electric-current pulse that heated them to a radiance temperature of about 1200 K at the shortest wavelength and about 765 K at the longest one, corresponding roughly to 1550 K in true temperature. Having been "pre-heated", each of these specimens remained in the argon-filled chamber for a few minutes (in order to secure the acquired data and reset the system) before finally being melted by a second and stronger pulse.

Well-formed melting plateaus were observed in all five melting experiments. In the case of the first specimen, however, the data of the first and third channels were lost due to a glitch in the data acquisition. The electric-current pulse, used to heat each specimen from room temperature to its melting point, ranged in amplitude from 462 to 476 A. The specimens reached their melting point in 621 to 635 ms, corresponding to average heating rates of 2.31 to 2.26 $K \cdot ms^{-1}$. The time from the onset of melting to the collapse of the partly liquid specimen, as indicated by the abrupt loss of electrical continuity and the resulting end of the quasi-rectangular current pulse, ranged from 108 to 133 ms. The number of temperature-data points along the plateau that were actually used for averaging ranged from 101 to 201, depending on the melting behavior of the specimen and on the wavelength. The standard deviation of an individual temperature-data point from the average plateau temperature of a specimen was less than 0.15 K at all wavelengths.

Figure 1 shows typical radiance temperature data just before and during melting. In all cases the onset of melting was manifested by a sharp increase in the measured radiances, which translated into a corresponding increase in the radiance temperatures. This was followed by a rather short plateau of about 5 to 10 ms, a decrease in radiance, and a second, longer plateau. Because of its better reproducibility, as can readily be seen in Fig. 2, it was the flat region along this second plateau that was used to determine the melting-point radiance temperature at each wavelength. The trend (or slope) of this flat region, as determined by least-squares fitting a linear function in time to the measured radiance temperatures, was in the range of -23 to $22\,K \cdot s^{-1}$ for all experiments. The temperature difference between the beginning and end of the flat part of the plateau, as determined from this slope, was in the range of -0.23 to 0.29 K.

5. RESULTS

The final results on the measured melting-point radiance temperatures and normal spectral emittances of nickel are presented in Table I and plotted as functions of wavelength in Figs. 3 and 4. The true melting

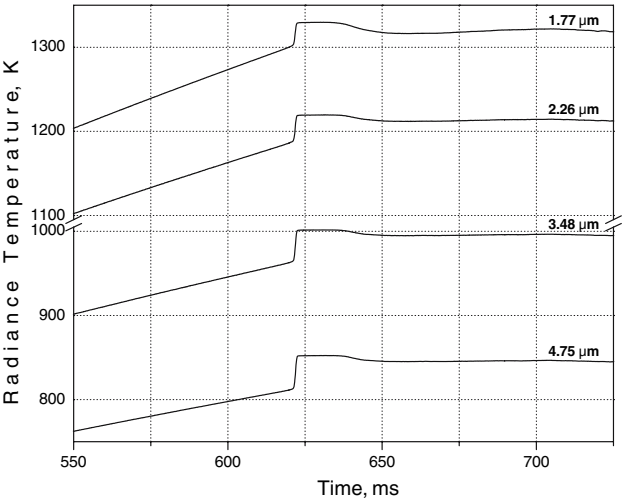

Fig. 1. Variation of the radiance temperature of a nickel specimen just before and during melting, as measured by the four-wavelength pyrometer. Onset of melting is manifested by a "kink" in the traces and a sharp increase in radiance thereafter.

temperature that was used in computing the normal spectral emittances was 1729 K (on ITS-90) [7].

Depending on the wavelength, the standard deviation of the average plateau radiance temperature of an individual specimen from the overall average of all specimens was in the range of 0.3 to 0.8 K. Similarly, depending on the wavelength, the maximum absolute deviation of the average plateau radiance temperature of an individual specimen from the overall average of all specimens was in the range of 0.4 to 1 K. Figure 5 shows the deviations of the average plateau radiance temperatures of the individual specimens from the final results.

The expanded uncertainty (coverage factor $k = 2$ and thus a two-standard-deviation estimate) of the reported melting-point radiance temperatures is 7 K for the shortest-wavelength channel, 6 K for the next two channels, and 5 K for the longest wavelength. The relative expanded uncertainty of the reported melting-point normal spectral emittances is 3.5% at the shortest wavelength, decreasing to about 2% at the longest one.

6. DISCUSSION

Because of the limited scope of our investigation, no effort was made to deliberately alter the initial surface roughness of the specimens or to

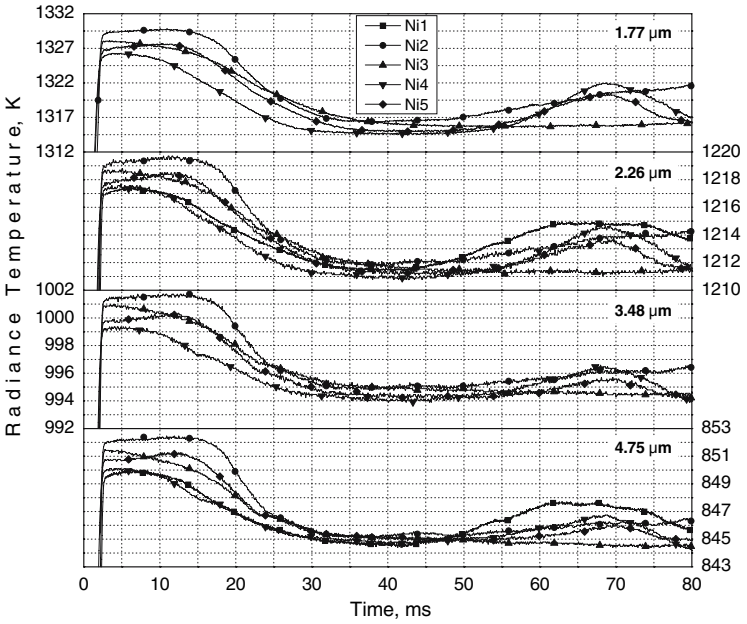

Fig. 2. Comparison of the melting behavior of the five nickel specimens. All traces were shifted in time, each by the appropriate amount, to make the onset of melting appear synchronous (in other words, time "zero" corresponds to the observed kink in the radiance traces).

vary any other experimental parameter, such as the heating rate, in order to study its effect on the measured melting-point radiance temperatures. The only exception was the application of a pre-heating pulse on three of the specimens, which was found to have no impact on the results.

Our measurements show that both the radiance temperature and the normal spectral emittance at the melting point of nickel decrease with increasing wavelength in the nominal range of 1.5 to 5 μm (Figs. 3 and 4). This finding is in agreement with previous work on this and other higher-temperature metals by the thermophysics laboratories of NIST and INRIM [10; 18].

The present radiance-temperature results agree remarkably well with the data previously reported by Kaschnitz et al. [8], when the latter are extrapolated to longer wavelengths. It should be stressed here, that although both measurement series were carried out at the same facility, not only do they span almost ten years, but also they were conducted by different researchers employing completely different pyrometers

Table I. Radiance Temperature $T_{\lambda,\mathrm{m}}$ and Normal Spectral Emittance $\varepsilon_{\lambda,\mathrm{m}}$ (at the respective Mean Effective Wavelengths $\lambda_{T_{\lambda,\mathrm{m}}-T_{\mathrm{ref}}}$ and $\lambda_{T_{\lambda,\mathrm{m}}-T_{\mathrm{m}}}$) of Nickel at its Melting Point of $T_{\mathrm{m}} = 1729\,\mathrm{K}$ (on ITS-90) [7]

$\lambda_{T_{\lambda,\mathrm{m}}-T_{\mathrm{ref}}}$ (nm)[a]	$T_{\lambda,\mathrm{m}}$ (K)	S.D. (K)[b]	Max. abs. dev. (K)[c]	$\lambda_{T_{\lambda,\mathrm{m}}-T_{\mathrm{m}}}$ (nm)[d]	$\varepsilon_{\lambda,\mathrm{m}}$ (-)	$\varepsilon_{\ell}/\varepsilon_{\mathrm{s}}$ (-)[e]
1774	1315.5	0.8	1	1771	0.227	1.13
2259	1211.4	0.4	0.6	2249	0.202	1.14
3484	994.5	0.4	0.5	3475	0.158	1.17
4755	844.9	0.3	0.4	4743	0.136	1.19

[a]Mean effective wavelength (as defined in Ref. [14]) between $T_{\lambda,\mathrm{m}}$ and the calibration temperature T_{ref}.
[b]Standard deviation of the average plateau radiance temperature of an individual specimen from the overall average of several specimens.
[c]Maximum absolute deviation of the average plateau radiance temperature of an individual specimen from the overall average of several specimens.
[d]Mean effective wavelength (as defined in Ref. [14]) between $T_{\lambda,\mathrm{m}}$ and the true melting temperature T_{m}.
[e]Ratio of the normal spectral emittance ε_{ℓ} of liquid nickel at the very onset of melting (not $\varepsilon_{\lambda,\mathrm{m}}$!) to that of solid nickel, ε_{s}, at the melting temperature.

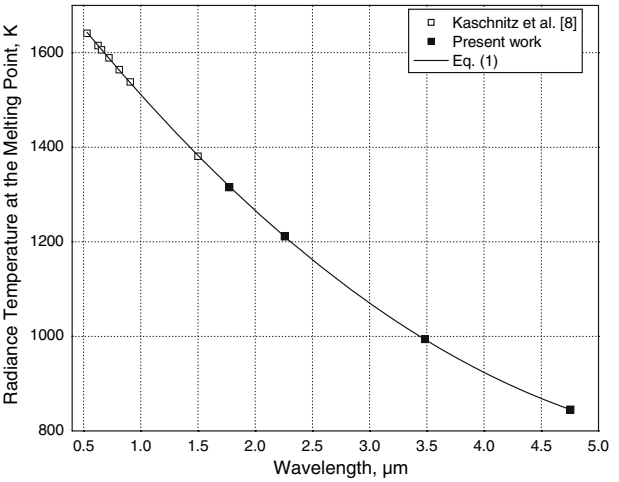

Fig. 3. Variation of the radiance temperature of nickel at its melting point as a function of wavelength.

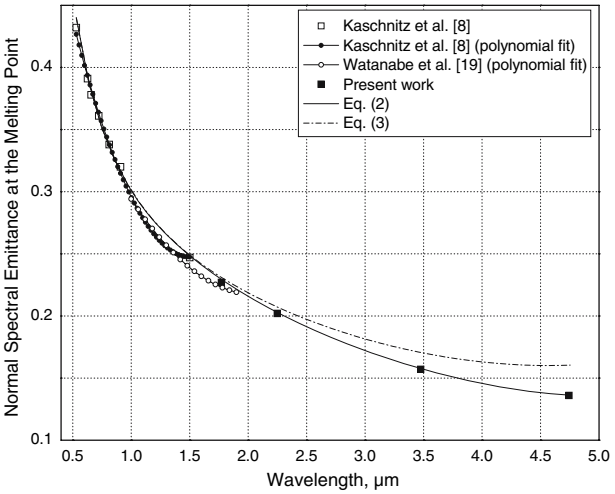

Fig. 4. Variation of the normal spectral emittance of nickel at its melting point as a function of wavelength.

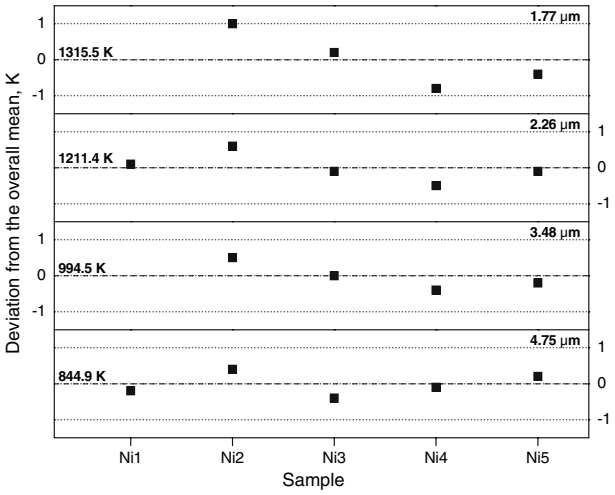

Fig. 5. Deviation of the measured radiance temperatures at the melting point of the individual specimens from the overall mean values (represented by the "zero" lines) at four wavelengths. The initial (prior to heating) normal spectral emittances of the specimens at 1.55 μm, as measured with our integrating-sphere reflectometer, were 0.244, 0.249, 0.249, 0.249, and 0.253 (from Ni1 to Ni5).

Table II. Coefficients of Eq. (1) for the Radiance Temperature $T_{\lambda,m}$ of Nickel at its Melting Point in the Wavelength Range of 0.53 to 4.76 μm

Coefficients		Exp. Uncertainty[a]
a	1804.9 K	2.7 K
b	-0.3183 K nm^{-1}	0.0031 K nm^{-1}
c	$2.449 \cdot 10^{-5}$ K nm^{-2}	$0.061 \cdot 10^{-5}$ K nm^{-2}
S.D.[b]	1.5 K	
Max. abs. dev.[c]	2 K	

[a]Expanded uncertainty with a coverage factor of $k=2$ and thus a two-standard-deviation estimate.
[b]Standard deviation of the least-squares fit.
[c]Maximum absolute deviation of the least-squares fit from a data point.

with different calibration procedures. This demonstrates the high degree of reproducibility that can be achieved using pulse-heating techniques.

The solid curve in Fig. 3 represents a least-squares fit of a quadratic function to both the present results and the earlier data by Kaschnitz et al. in their combined wavelength range of 0.53 to 4.76 μm. It is of the form,

$$T_{\lambda,m} = a + b\lambda + c\lambda^2 \tag{1}$$

where $T_{\lambda,m}$ and λ stand for the melting-point radiance temperature and the wavelength, respectively. The values of the three coefficients are given in Table II.

Similarly, in Fig. 4 we plot both the present results and those obtained earlier by Kaschnitz et al. for the normal spectral emittance of nickel at its melting point. Despite the good agreement, however, in this case it was impossible to find a polynomial that described all measurements (present and previous) satisfactorily over the entire wavelength range. In fact, even the quadratic function reported by Kaschnitz et al. in the narrower range of 0.53 to 1.5 μm, although a good fit in terms of its standard deviation, becomes problematic at wavelengths above 1 μm (Fig. 4). Its minimum lies very close to the endpoint at 1.5 μm, so that an extrapolation of only a few nanometers to longer wavelengths quickly results in a positive slope, contradicting the generally observed behavior of the normal spectral emittance of metals at their melting points.

Instead, we got a much better fit to the data by expressing the emittance as a function of wavelength using Planck's law and the already computed function for the radiance temperature (Eq. (1));

$$\varepsilon_{\lambda,\mathrm{m}} = \frac{\exp\left(\frac{c_2}{\lambda T_\mathrm{m}}\right) - 1}{\exp\left[\frac{c_2}{\lambda(a+b\lambda+c\lambda^2)}\right] - 1} \tag{2}$$

where $\varepsilon_{\lambda,\mathrm{m}}$ is the melting-point normal spectral emittance, T_m is the true melting temperature, and $c_2 = 14388\,\mu\mathrm{m\,K}$ is Planck's second radiation constant. This equation is plotted in Fig. 4 as a solid curve in the range of 0.53 to 4.76 μm. Its standard deviation from the data is 0.0033, whereas its maximum absolute deviation from any data point is 0.008 (less than 2%). The dashed-dotted line in Fig. 4 represents the same equation according to Wien's law;

$$\ln \varepsilon_{\lambda,\mathrm{m}} = \frac{c_2}{\lambda}\left(\frac{1}{T_\mathrm{m}} - \frac{1}{a+b\lambda+c\lambda^2}\right) \tag{3}$$

Its deviation from Eq. (2) reaches 1% at around 1.9 μm. It was included here as a visual reminder that whenever Wien's law is used (often only indirectly, as part of the derivation of some other expression), it is necessary to check that the product of $\lambda \cdot T$ does not exceed some critical value, which is set by the required accuracy. In the case of Eq. (2), for instance, the value of $3100\,\mu\mathrm{m\,K}$ (at which Wien deviates from Planck by 1%) is exceeded at roughly 1.8 μm in the numerator and 2.8 μm in the denominator. This is something that is easily overlooked in high-temperature work, where the pyrometer wavelengths involved are shorter, typically in the visible region.

Also plotted in Fig. 4 are the results of Watanabe et al. [19] for the normal spectral emittance of liquid nickel at its melting point in the range of 1 to 1.9 μm. At 1.77 μm they differ from our data point by 0.004 or less than 2%. The deviation from Eq. (2) varies between 1% (at 1.9 μm) and a little under 4% (at 1.5 μm).

As with tin, zinc, aluminum, and silver [5], the most interesting feature that we observed in the melting behavior of the nickel specimens was the already mentioned sharp increase in the measured radiances at the onset of melting (Fig. 1). For reasons that were laid out in Ref. [5], we believe that this increase is due to intrinsic differences between the solid and liquid phases. Therefore, it is a direct measure of the change in the normal spectral emittance of nickel as it undergoes the phase transition. The liquid-to-solid signal ratios at the four pyrometer wavelengths are listed in Table I. They indicate that the relative emittance change upon melting increases monotonically with increasing wavelength. It is important to note that the "liquid signal" used to compute these ratios was the signal along the first (and shorter) melting sub-plateau mentioned earlier in this paper (Figs. 1 and 2). This was higher than the signal along

the following longer and more reproducible plateau, which was used to compute the melting-point radiance temperatures and emittances. Presumably, in the initial stages of melting, the liquid specimen surface retains its roughness from the solid state (at least to some degree, therefore having a higher emittance) before ultimately smoothening due to surface tension. This is supported by the fact that the signal ratio of the first to the second (and lower) sub-plateau is largest in the shortest-wavelength channel, which should be more sensitive to the existence of surface roughness.

Watanabe et al. [19; 20; 21] have studied the phase dependence (liquid/solid) of the melting-point normal spectral emittance of several metals, including nickel, in the visible and near-infrared regions. In the case of nickel, their result in the liquid-to-solid emittance ratio at 1.77 μm is about 1% higher than our measurement. The agreement is exceptionally good, considering that whereas our measurements of this ratio probably include the effect of some surface roughness, their measurements were taken during the freezing transition of previously molten specimens, and thus on very clean, smooth surfaces by virtue of the re-solidification process. It is as though, in our case, the effect of roughness on the specimen emittance is that of a multiplicative factor, which is cancelled out when forming the ratio of the two values (liquid/solid). This could be of value for other kinds of experiments as well, such as in shock physics, where rapid melting takes place and in which the emittance in the liquid needs to be estimated from that in the solid for pyrometric use.

From a scientific point of view, the change of the emittance of a metal upon melting is important because it is related to the electronic structure of the liquid and solid phases. In Ref. [5] we suggested comparing the measured emittance increase to that predicted from the corresponding resistivity change by means of the simple Hagen–Rubens relation. As it turns out, Watanabe et al. have already obtained good results by applying various models (including Hagen–Rubens) to the solid and liquid emittances of several metals, including nickel, mostly at shorter wavelengths. We plan to adapt their approach with our data on tin, zinc, aluminum, silver, and nickel at the longer wavelengths, where modeling should be simpler.

REFERENCES

1. K. Boboridis and A. W. Obst, *Temperature: Its Measurement in Science and Industry*, Vol. 7, Part 2, D.C. Ripple, ed. (AIP, New York, 2003), p. 759.
2. A. Seifter, K. Boboridis, D. A. Clark, R. B. Corrow, D. B. Holtkamp, C. W. McCluskey, G. L. Morgan, J. R. Payton, P. Quintana, C. E. Ragan, P. Rodriguez, H. L. Stacy, W. S. Vogan, V. W. Yuan, and A. W. Obst, in *Proc. 9th Int. Symp. on Temperature and Thermal Measurements in Industry and Science (TEMPMEKO)*, Vol. 2 (2004), p. 1185.

3. A. Seifter, S. T. Stewart, M. R. Furlanetto, G. B. Kennedy, J. R. Payton, and A. W. Obst, *Shock Compression of Condensed Matter – 2005*, M. D. Furnish, M. Elert, T. P. Russell, and C. T. White, eds. (AIP, New York, 2006).
4. K. Boboridis, A. Seifter, and A. W. Obst, *VDI Berichte* **1784**:119 (2003).
5. K. Boboridis, A. Seifter, A. W. Obst, and D. Basak, *Int. J. Thermophys.* **25**:1187 (2004).
6. K. Boboridis, A. Seifter, A. W. Obst, and D. Basak, presented at the *15th Symp. Thermophys. Props.*, Boulder, Colorado (2003).
7. A. Cezairliyan and A. P. Miiller, *Int. J. Thermophys.* **5**:315 (1984).
8. E. Kaschnitz, J. L. McClure, and A. Cezairliyan, *Int. J. Thermophys.* **19**:1637 (1998).
9. A. Cezairliyan, A. P. Miiller, A. Righini, and A. Rosso, in *Temperature: Its Measurement and Control in Science and Industry*, Vol. 5, Part 1, J. F. Schooley, ed. (AIP, New York, 1982), p. 377.
10. A. Cezairliyan, A. P. Miiller, A. Righini, and A. Rosso, in *Temperature: Its Measurement and Control in Science and Industry*, Vol. 6, Part 1, J. F. Schooley, ed. (AIP, New York, 1992), p. 377.
11. A. Cezairliyan, M. S. Morse, H. A. Berman, and C. W. Beckett, *J. Res. Natl. Bur. Stand. (US)* **74A**:65 (1970).
12. A. Cezairliyan, *J. Res. Natl. Bur. Stand. (US)* **75C**:7 (1971).
13. T. Matsumoto and A. Cezairliyan, *Int. J. Thermophys.* **18**:1539 (1997).
14. H. J. Kostkowski and R. D. Lee, in *Temperature: Its Measurement and Control in Science and Industry*, Vol. 3, Part 1, C. M. Herzfeld, ed. (Reinhold, New York, 1962), p. 449.
15. H. Preston-Thomas, *Metrologia* **27**:3 (1990); *Metrologia* **27**:107 (1990).
16. A. Seifter, K. Boboridis, and A. W. Obst, *Int. J. Thermophys.* **25**:547 (2004).
17. E. Fromm, *Metall. Trans.* **9A**:1835 (1978).
18. A. Cezairliyan, A. P. Miiller, F. Righini, and A. Rosso, *High Temp. High Press.* **23**:325 (1991).
19. H. Watanabe, M. Susa, H. Fukuyama, and K. Nagata, *Int. J. Thermophys.* **24**:473 (2003).
20. H. Watanabe, M. Susa, H. Fukuyama, and K. Nagata, *Int. J. Thermophys.* **24**:223 (2003).
21. H. Watanabe, M. Susa, H. Fukuyama, and K. Nagata, *Int. J. Thermophys.* **24**:1105 (2003).